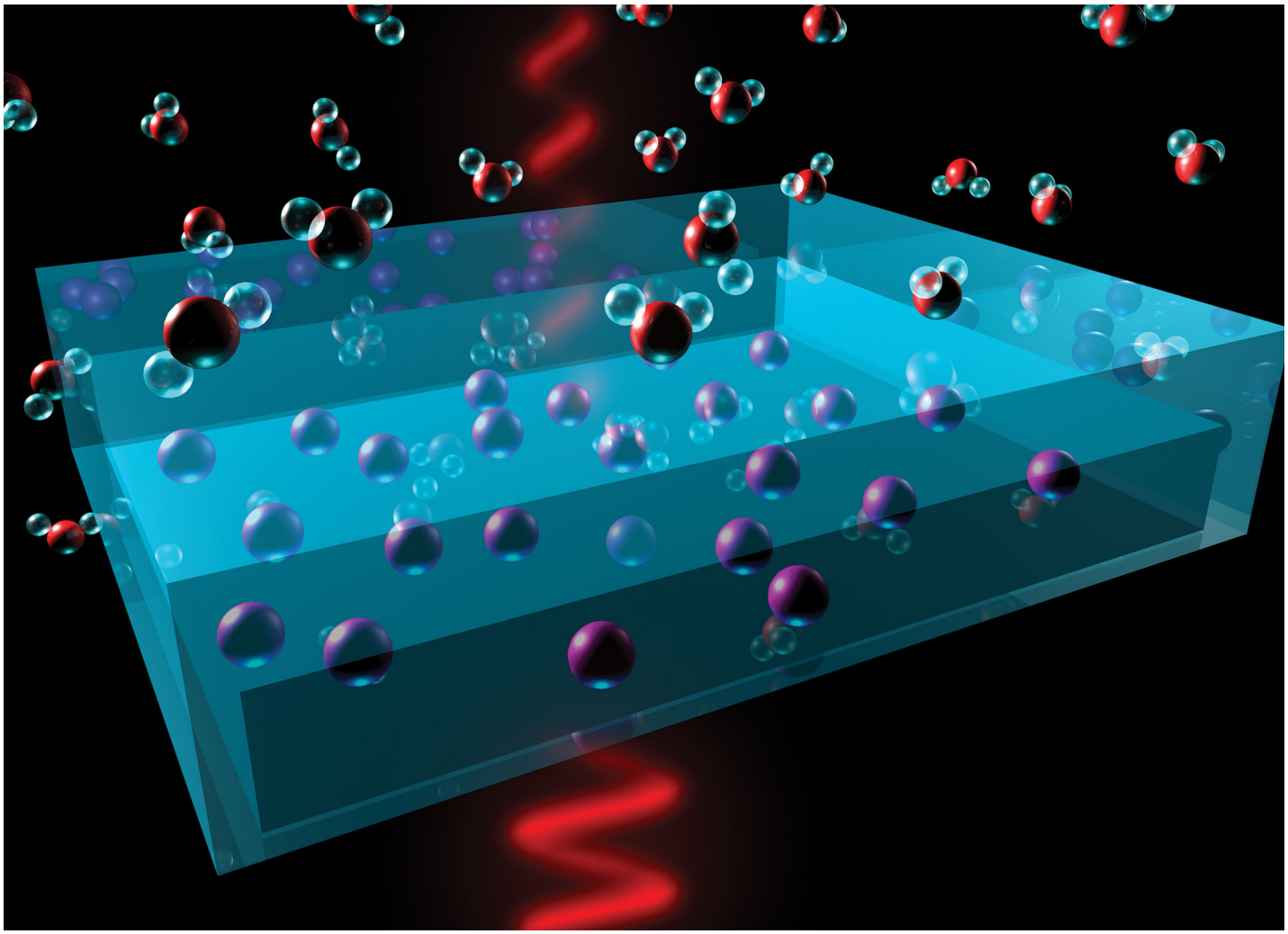

Highlighting research performed in the group of Prof. Olga Kuksenok in collaboration with Konstantin Kornev from Clemson University.

Controlling deformations of gel-based composites by electromagnetic signals within the GHz frequency range

Savchak *et al*. use computational modelling to design gel-based composites undergoing large deformations under an application of electromagnetic signals within the GHz frequency range. When the frequency of the signal is close to that of the Ferro-Magnetic Resonance frequency, the heating rate increases dramatically and the composite undergoes volume phase transitions. Hence, the mechanical response of the sample is controlled by the external electromagnetic signal and is highly selective. Designing soft materials that can be actuated by the electromagnetic signals within the GHz frequency range is of particular interest given an extensive use of the GHz bands in various communication protocols. Artwork by Mykhailo Savchak and Oksana Savchak.

As featured in:

See Olga Kuksenok *et al*., *Soft Matter*, 2018, **14**, 8698.

ROYAL SOCIETY OF CHEMISTRY

rsc.li/soft-matter-journal

Registered charity number: 207890

Soft Matter

PAPER

View Article Online
View Journal | View Issue

Cite this: *Soft Matter*, 2018, **14**, 8698

Controlling deformations of gel-based composites by electromagnetic signals within the GHz frequency range†

Oksana Savchak,[a] Tyler Morrison,[b] Konstantin G. Kornev[a] and Olga Kuksenok*[a]

Received 13th June 2018,
Accepted 30th September 2018

DOI: 10.1039/c8sm01207e

rsc.li/soft-matter-journal

Using theoretical and computational modeling, we focus on dynamics of gels filled with uniformly dispersed ferromagnetic nanoparticles subjected to electromagnetic (EM) irradiation within the GHz frequency range. As a polymer matrix, we choose poly(*N*-isopropylacrylamide) gel, which has a low critical solution temperature and shrinks upon heating. When these composites are irradiated with a frequency close to the Ferro-Magnetic Resonance (FMR) frequency, the heating rate increases dramatically. The energy dissipation of EM signals within the magnetic nanoparticles results in the heating of the gel matrix. We show that the EM signal causes volume phase transitions, leading to large deformations of the sample for a range of system parameters. We propose a model that accounts for the dynamic coupling between the elastodynamics of the polymer gel and the FMR heating of magnetic nanoparticles. This coupling is nonlinear: when the system is heated, the gel shrinks during the volume phase transition, and the particle concentration increases, which in turn results in an increase of the heating rates as long as the concentration of nanoparticles does not exceed a critical value. We show that the system exhibits high selectivity to the frequency of the incident EM signal and can result in a large mechanical feedback in response to a small change in the applied signal. These results suggest the design of a new class of soft active gel-based materials remotely controlled by low power EM signals within the GHz frequency range.

1. Introduction

The ability of many organisms to sense magnetic fields, a phenomenon known as magnetoreception, is often vital for their functionality. Designing soft synthetic materials capable of adjusting their functionality in response to variations in applied magnetic fields would be advantageous for the development of a range of remotely controlled soft coatings, sensors, and actuators. Controlling the dynamics of these materials by low power electromagnetic (EM) signals within the GHz frequency range is of particular interest given the extensive usage of GHz bands in various communication protocols. For example, Bluetooth technologies operate at 2.4 GHz and 5 GHz frequencies while Metropolitan Area Network (MAN) protocols and radars operate within a broader range of GHz bands.[1] Developing soft active reconfigurable materials that would ultimately allow one to control mechanical actuation, shape, or wetting properties through the usage of the existing communication protocols could be beneficial for a range of applications.

Harnessing nonlinear coupling between electromagnetic waves and elastic deformations, such as those observed in recently proposed metamaterials,[2,3] is a promising direction in the development of soft active materials. To date, significant progress has been made in understanding the behaviour of magnetic gels or ferrogels in uniform[4–9] and nonuniform[10] DC magnetic fields. Herein, we focus on the design of soft gel-based magnetic composites formed by a thermo-responsive hydrogel matrix filled with ferromagnetic nanoparticles. The goal is to identify the conditions leading to large elastic deformations upon electromagnetic heating of these composites within the GHz frequency range. The key feature of these systems is that the magnetic heating is nonlinearly coupled with the gel's dynamics resulting in a large-scale deformation of the composite in response to a relatively small variation of the applied EM signal.

As a polymer matrix, we choose poly(*N*-isopropylacrylamide) (PNIPAAm) gel. PNIPAAm polymers have a lower critical solution temperature (LCST), and hence PNIPAAm gels shrink upon heating above the volume phase transition temperature.[11] We consider single-domain ferromagnetic nanoparticles (NPs) uniformly dispersed within the matrix similar to the system

[a] *Materials Sciences and Engineering, Clemson University, Clemson, SC, 29634, USA. E-mail: okuksen@clemson.edu*
[b] *Department of Mechanical and Aerospace Engineering, The Ohio State University, Columbus, OH, 43210, USA*

† Electronic supplementary information (ESI) available. See DOI: 10.1039/c8sm01207e

considered in ref. 12. These NPs could be either covalently grafted onto the polymer network or physically trapped within it so that they move together with the polymer matrix (similarly to two types of magnetic gel fabricated in ref. 13). To prevent aggregation of the nanoparticles within the gel during the sample preparation, these NPs could be coated to ensure compatibility with the gel matrix.[14] As we show below, when these composites are subjected to EM irradiation with a frequency close to the Ferro-Magnetic Resonance (FMR) frequency, the absorbance of the samples increases, driving the gels through the volume phase transition. This, in turn, results in a dynamic variation of the resonance frequency. We consider only low concentrations of the nanoparticles (initial concentrations are varied between 0.5% and 1% in the simulations below) and it is assumed that the nanoparticles move together with the polymer matrix. We note that at higher concentrations of nanoparticles, magnetic gels were also shown to undergo deformations in the uniform magnetic fields. For example, molecular dynamic simulations of the gel network with every second nanoparticle in the chain having a magnetic moment, placed on the two-dimensional lattice, showed two distinct modes of deformation of the network and the formation of magnetic chains.[5] Furthermore, experimental studies showed up to 2% elongation of a ferrogel sphere in a homogeneous magnetic field.[15] Herein, we solely focus on magnetic gels with low concentration of nanoparticles placed within thermoresponsive hydrogels and hence do not consider any deformations of the matrix in the absence of the applied EM wave. The electromagnetic wave is partially adsorbed by the sample resulting in the heating of the composite; any deformations of the matrix in the absence of the applied EM wave are assumed to be insignificantly smaller than those caused by the EM heating.

A number of prior studies have demonstrated the efficiency of heating of hydrogels filled with superparamagnetic nanoparticles.[13,16–19] In these studies, a typical frequency of the EM signal is on the order of hundreds of kHz and the heating mechanism is due to the combination of the flipping of spins called Neel's relaxation and viscous dissipation due to the Brownian motion of NPs in the matrix.[20,21] The applications of these hydrogels filled with magnetic nanoparticles range from biomedical drug delivery for hyperthermia treatments[22,23] to utilizing external EM signals for the remote control of hydrogel membrane porosity for the well-targeted molecular sieving.[24] Either PNIPAAm gels[25,26] or various copolymers[27,28] are used in the studies of hydrogel–magnetic nanoparticle composites.

Herein, we focus on the GHz frequency bands, where the mechanism of gel heating is distinctly different.[12,29] The heating rates calculated for non-deformable composites such as paraffin films filled with various magnetic nanoparticles at GHz frequencies[12] support the feasibility of using these frequencies to control the volume phase transitions in thermo-responsive hydrogels. With respect to the hydrogels filled with ferromagnetic nanoparticles considered here, we isolate the effects of magnetic heating caused by the interaction of the EM wave with ferromagnetic NPs, neglecting dielectric losses within the hydrogel matrix. While water is well known to absorb effectively within the GHz frequency band[30] and would result in dielectric losses within the gel matrix, magnetic nanoparticles dispersed within soft matrices are shown to significantly enhance the localized selective microwave heating,[31,32] providing significantly greater contribution from the magnetic heating than from the corresponding dielectric losses.[31] To further isolate the effects of magnetic heating and minimize dielectric losses in the PNIPAAm films filled with magnetic nanoparticles, these films could be placed on a metal substrate in the respective experiments; for thin films with a thickness significantly smaller than the wavelength of the EM wave, the electric component of the EM wave will be reflected from the metal.‡[33]

Herein, we develop a model that couples heating within the GHz frequency range in gel–magnetic nanoparticle composites with the gel elastodynamics in three dimensions. We then focus on the mechanical response of these composites to the applied EM waves. In the simulations below, we only focus on heating of the samples and assume that the sample along with the solvent it is immersed in is thermally insulated. The thermal diffusivity of water (1.4×10^{-7} m^2 s^{-1}) is a few orders of magnitudes higher than the collective diffusion coefficient of the polymer network[34] (taken as[35] 2×10^{-11} m^2 s^{-1} in the estimates below). Consequently, we assume that the temperature is equilibrated instantaneously and is uniform within the gel sample[34] at any given moment in time for the sample sizes considered in this work.

2. Model: M-gLSM

We first develop a model that couples the FMR heating of magnetic nanoparticles with the gel elastodynamics. We model gel elastodynamics based on the gel Lattice Spring Model (gLSM).[36–38] Originally, the gLSM[36–38] was developed to simulate the dynamics of self-oscillating gels undergoing the Belousov–Zhabotinsky chemical reactions[39] and combines a finite element approach for the spatial discretization of the equations of the gel dynamics and a finite difference approximation for modeling reaction–diffusion equations. The findings from a number of computational studies using the gLSM are in good agreement with the corresponding experimental results,[36,40–43] making this approach an effective tool for simulating the dynamics of various chemo-responsive gels. In this work, we adapt a three-dimensional gLSM framework[36] to simulate the effects of interactions of the EM wave and a gel composite filled with magnetic nanoparticles; we will refer to this framework as M-gLSM.

The schematic of our system is shown in Fig. 1. A gel layer filled with magnetic nanoparticles is subjected to a bias magnetic field ($\mathbf{H}_{ex}$), while an EM wave with the magnetic field $\mathbf{h}_0$

‡ For example, for the wave with the wavelength of 2.3 cm (12.6 GHz), the maximum electric field is expected to be at ~0.57 cm away from the metal surface[26] covered with the gel layer. Hence for the composite films that are significantly thinner than the quarter wavelength (the thickness is set at approximately 5 μm in the simulations below), one can neglect the dielectric loses within the film.

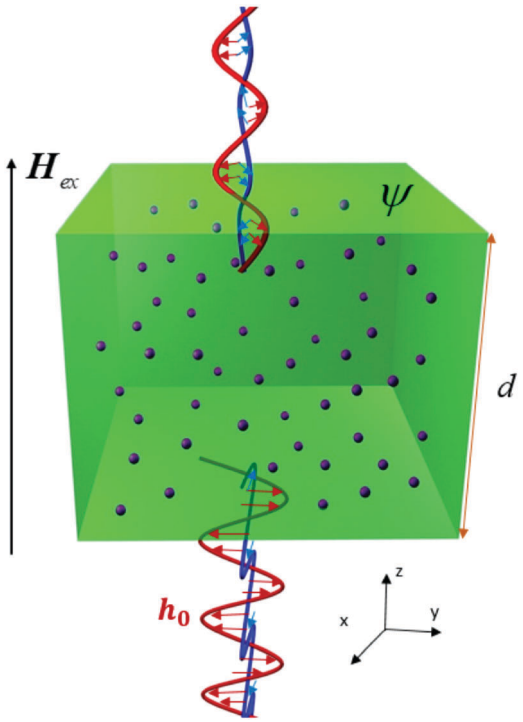

Fig. 1 Schematic of the gel composite under the FMR heating. A gel layer filled with magnetic nanoparticles is subjected to a bias magnetic field, $\mathbf{H}_{ex}$, and an EM wave with the magnetic field $\mathbf{h}_0$ perpendicular to $\mathbf{H}_{ex}$ is applied in the z-direction. Nanoparticles are assumed to be uniformly distributed and trapped within the gel matrix.

perpendicular to $\mathbf{H}_{ex}$ is applied (in red in Fig. 1). When an applied frequency coincides with the natural precession frequency of the magnetic composite, maximum absorption is observed; this phenomenon is known as ferromagnetic resonance (FMR).[44] The corresponding experimental setup includes an EM wave excitation source, a permanent electromagnet, and a detector. To observe the resonance conditions, one could either vary the strength of the external field keeping the applied frequency of the EM wave fixed or scan over a range of frequencies keeping the external field fixed. In our simulations, we keep $\mathbf{H}_{ex}$ constant and vary the frequency of the EM signal.

We only consider low concentrations of the nanoparticles (initial concentrations do not exceed 1% in the simulations below), thereby neglecting interactions between the nanoparticles.[12] At a known instantaneous value of volume fraction of nanoparticles, ψ, and a known instantaneous thickness of the gel layer, d, we calculate the instantaneous heating rate using an approach developed in ref. 12. During the application of the EM irradiation, the thickness d and the volume fraction of the nanoparticles ψ vary with time as the sample is deformed due to heating.

To capture the elastodynamics of the composite within the M-gLSM framework, at each instant of time we calculate (1) the instantaneous heating rate[12] that depends on the gel thickness, d, and the volume fraction of the nanoparticles, ψ, (2) the instantaneous temperature, T, of the sample based on this heating rate and the temperature of the sample at a previous moment of time; and (3) the polymer–solvent interaction parameter that depends on temperature[11] and defines the degree of swelling of the gel as given below. Lastly, in step (4), we perform the integration of the elastodynamics equations (3D gLSM) using this calculated polymer–solvent interaction parameter. Hence, the M-gLSM framework allows one to account for the effects of interactions of the electromagnetic wave and the gel composite filled with ferromagnetic nanoparticles and for the coupling between the magnetic heating and the mechanical response of the gel matrix. For simplicity here, we consider only small cubic gel samples freely suspended within the solvent.[36] Note that modeling larger samples (grafted onto the substrate or under various confinements) would be a straightforward extension of the proposed M-gLSM approach. The initial temperature of the system sets the initial equilibrium degree of swelling of gel (in the absence of an applied electromagnetic signal) and thereby sets the initial equilibrium dimensions of the sample.[36]

2.1 Calculating heating rates

In the case of a non-deformable composite filled with NPs at a constant volume fraction of nanoparticles, ψ, and a constant layer thickness, d, the heating rate of the sample as a function of EM wave frequency and applied magnetic field was calculated as in ref. 12. Assuming that the easy axes of the nanoparticles are oriented parallel to the external bias magnetic field (along the positive z-direction in Fig. 1), the magnetic field within the gel film can be determined as:[12]

$$\mathbf{H}_{in} = \mathbf{H}_{ex} - \psi\mathbf{M}, \quad (1)$$

where $\mathbf{M}$ is the magnetization vector of the single nanoparticle. In the absence of the EM wave, the magnetic moments of nanoparticles would orient along the bias field within the nanoparticle, $\mathbf{H}_s$ (in a vertical direction in Fig. 1), which for the spherical nanoparticles can be written as:[12]

$$\mathbf{H}_s = \mathbf{H}_{in} + \left(\frac{2K_1}{\mu_0 M_s} - \frac{M_s}{3}\right)\mathbf{z}, \quad (2)$$

where M_s is the saturation magnetization of the material, K_1 is a constant of magnetocrystalline anisotropy,[44] μ_0 is the permeability of a vacuum, and $\mathbf{z}$ is the unit vector along the vertical direction in Fig. 1. The application of the EM wave destabilizes the magnetization of the NPs along the $\mathbf{H}_s$, causing precession of the magnetization vector. The dynamics of the magnetization vector can be described by the Landau–Lifshitz–Gilbert equation,[29,33] which introduces a phenomenological Gilbert damping coefficient α, accounting for energy dissipation within the nanoparticles due to the combined contributions of various effects (from the coupling between the magnetization fields and lattice vibrations to the energy dissipation due to the defects in crystalline structures[29]).

The resonance frequency of the composite depends on the magnitude of the external biased magnetic field, the magnetic properties of the nanoparticles (such as magnetocrystalline anisotropy and saturation magnetization, gyromagnetic ratio γ and phenomenological damping coefficient α), and the

volume fraction of the nanoparticles within the composite, ψ. This resonance frequency can be written as:[12]

$$w_c = \gamma\mu_0\left(|\mathbf{H}_{ex}| - \psi M_s + \frac{2K_1}{\mu_0 M_s}\right). \quad (3)$$

For the given thickness of the sample and a volume fraction of the nanoparticles, the instantaneous heating rate of the composite reads:[12]

$$K_T = \frac{P_0\eta(\tilde{w},\psi)}{\rho c_p d}, \quad (4)$$

where P_0 is the power density per unit area (measured in W m^{-2}), ρ is the density of the composite, c_p is the specific heat capacity and d is the thickness of the sample in the direction perpendicular to the incident EM wave. In eqn (4), the absorption coefficient, η, that characterizes the ratio of the energy absorbed by the composite of the thickness d to the energy pumped into the system is defined as:

$$\eta = 1 - T(\tilde{w},\psi) - R(\tilde{w},\psi), \quad (5)$$

where the transmission coefficient, T, is the ratio of intensity transmitted to the intensity incident and the reflection coefficient, R, is the ratio of intensity reflected to the intensity incident.[45] These values are calculated as:[12]

$$T(\tilde{w},\psi) = \left\{\frac{4e^{-ik_1 d}Z(\tilde{w},\psi)}{(Z(\tilde{w},\psi)-1)^2 e^{-2ik_1 d}Z(\tilde{w},\psi) - (Z(\tilde{w},\psi)+1)^2}\right\}^2, \quad (6)$$

$$R(\tilde{w},\psi) = \left\{\frac{\left(Z(\tilde{w},\psi)^2-1\right)\left(e^{-2ik_1 d}-1\right)}{(Z(\tilde{w},\psi)-1)^2 e^{-2ik_1 d} - (Z(\tilde{w},\psi)+1)^2}\right\}^2. \quad (7)$$

In eqn (6) and (7), the dimensionless frequency of the EM wave is defined as $\tilde{w} = w/w_r$, where $w_r = \gamma\mu_0|\mathbf{H}_{ex}|$, $Z(\tilde{w},\psi)$ is the ratio between the wave impedances in the composite and vacuum,

$$Z(\tilde{w},\psi) = \sqrt{\mu_{eff}(\tilde{w},\psi)/\varepsilon_{eff}}, \quad (8)$$

and the magnitude of the wave vector propagating through the composite is given by:

$$k_1 = w\sqrt{\varepsilon_0\mu_0\varepsilon_{eff}}\sqrt{\mu_{eff}(\tilde{w},\psi)}. \quad (9)$$

The effective magnetic permeability of the medium in eqn (8) and (9) is expressed as:[12]

$$\mu_{eff}(\tilde{w},\psi) = \left(1 + 3\psi\frac{\mu+g-1}{\mu+g+2}\right), \quad (10)$$

where μ and g are calculated as:

$$\mu(\tilde{w}) = 1 + \tilde{w}_m\frac{1+i\alpha\tilde{w}}{(1+i\alpha\tilde{w})^2 - \tilde{w}^2}, \quad (11)$$

$$g(\tilde{w}) = \frac{\tilde{w}_m\tilde{w}}{(1+i\alpha\tilde{w})^2 - \tilde{w}^2}, \quad (12)$$

with $\tilde{w}_m = \gamma\mu_0 M_s/w_r$.

In our model, the heating induced by the applied EM irradiation raises the temperature and decreases the volume of the sample. Correspondingly, the instantaneous heating rate varies with the variations in the sample thickness, d, and the volume fraction of the nanoparticles, ψ. Both of these values depend on the volume fraction of the polymer, φ, and thus are time-dependent for the gel composite. As the gel undergoes volume phase transition, the sample volume decreases and, correspondingly, the volume fraction of the nanoparticles, ψ, increases while d decreases. An effective magnetic permeability of the sample varies correspondingly (eqn (10) above) and is accounted for within the M-gLSM framework through the respective contributions to the absorption coefficient (eqn (5)). As noted above, the nanoparticles are considered to be grafted to (or physically trapped within) the polymer matrix and are assumed to move together with this matrix. We thereby calculate the fraction of nanoparticles, ψ, as $\xi_m\varphi$, where parameter ξ_m sets up the initial fraction of nanoparticles grafted onto the polymer matrix.

2.2 Modeling gel elastodynamics

Within the gLSM,[36–38] the total energy of chemo-responsive gels is taken as the sum of energy of the polymer–solvent interactions, U_{FH}, and elastic energy associated with the gel deformations, U_{el}. The first contribution is written in the following Flory–Huggins form:[46]

$$U_{FH} = \sqrt{I_3}[(1-\varphi)\ln(1-\varphi) + \chi_{FH}(\varphi,T)\varphi(1-\varphi)]. \quad (13)$$

Here, φ is the volume fraction of the polymer, $1-\varphi$ is the volume fraction of the solvent, and χ_{FH} is the Flory–Huggins polymer–solvent interaction parameter. Finally, $I_3 = \det\hat{\boldsymbol{B}}$ in eqn (13) is an invariant of the left Cauchy–Green (Finger) strain tensor $\hat{\boldsymbol{B}}$, which is related to the volume changes of the deformed gel.[47] The elastic energy contribution to the total energy, U_{el}, describes the rubber elasticity of the cross-linked network,[46,48] and is proportional to the crosslink density, c_0:

$$U_{el} = \frac{c_0 v_0}{2}\left(I_1 - 3 - \ln I_3^{1/2}\right), \quad (14)$$

where v_0 is the volume of the monomeric unit and $I_1 = \mathrm{tr}\,\hat{\boldsymbol{B}}$.[47] The constitutive equation for the chemo-responsive gels reads:[37]

$$\hat{\boldsymbol{\sigma}} = -P(\varphi,T)\hat{\boldsymbol{I}} + c_0 v_0\frac{\varphi}{\varphi_0}\hat{\boldsymbol{B}}, \quad (15)$$

where $\hat{\boldsymbol{\sigma}}$ is the dimensionless stress tensor measured in units of $v_0^{-1}kT$, $\hat{\boldsymbol{I}}$ is the unit tensor, φ_0 is the volume fraction of the polymer at preparation, and $P(\varphi,T)$ is the isotropic pressure defined as[11,37]

$$P(\varphi,T) = -\left(\varphi + \ln(1-\varphi) + \chi(\varphi,T)\varphi^2\right) + c_0 v_0\varphi(2\varphi_0)^{-1}. \quad (16)$$

The parameter $\chi(\varphi,T)$ in the above equation is a function of both polymer volume fraction, φ, and temperature, T, and is determined as:[11]

$$\chi(\varphi,T) = \chi_0(T) + \chi_1\varphi, \quad (17)$$

where

$$\chi_0(T) = [\delta h - T\delta s]/kT, \quad (18)$$

with δh and δs being the respective changes in the enthalpy and entropy per monomeric unit of the gel. In this elastomagnetic composite, the absorption of the EM wave results in the heating of the sample, which in turn leads to the dependence of $\chi_0(T)$ on the EM wave frequency and the respective changes in the equilibrium degree of swelling. This equilibrium degree of swelling as a function of temperature is determined as[36]

$$\lambda_{eq}(T) = (\varphi_0/\varphi_{eq}(T))^{1/3}, \quad (19)$$

where the equilibrium volume fraction of the polymer, $\varphi_{eq}(T)$, for an unconstrained three dimensional sample is found by requiring $\hat{\boldsymbol{\sigma}} = 0$ (eqn (15)) in equilibrium:[36]

$$c_0 v_0 \left[\left(\frac{\varphi_{eq}}{\varphi_0}\right)^{1/3} - \frac{\varphi_{eq}}{2\varphi_0}\right] = -\left(\varphi_{eq} + \ln\left(1-\varphi_{eq}\right) + \left[\chi_0(T) + \chi_1\varphi_{eq}\right]{\varphi_{eq}}^2\right). \quad (20)$$

The details of the three-dimensional formulation and implementation of the gLSM approach are provided in ref. 36.

2.3 Simulation parameters and their relationship to the experimental values

In the simulations below, we choose the reference parameters based on the following available experimental values. The reference parameters for the nanoparticles are chosen for the single domain cobalt (Co) nanoparticles taking the saturation magnetization and the magnetocrystalline anisotropy as M_s = 1.44×10^6 A m^{-1} and $K_1 = 4.5 \times 10^5$ J m^{-3}, respectively.[12] Hence, we use the following reference values: $w_m/2\pi = \gamma\mu_0 M_s/2\pi$ (taking the gyromagnetic ratio as 2×10^{11} rad T^{-1} s^{-1} and the magnetic permeability of the vacuum as $\mu_0 \approx 1.257 \times 10^{-6}$ H m^{-1} and $w_r/2\pi = {w_r}^0/2\pi - w_m/2\pi$, where ${w_r}^0/2\pi = \gamma\mu_0/2\pi(|\mathbf{H}_{ex}| + (2K_1/\mu_0 M_s) - M_s/3)$ is independent of the nanoparticle concentration). Taking $\mu_0|\mathbf{H}_{ex}| = 0.29$ T in the reference case, we set ${w_r}^0/2\pi = 10$ GHz. Note that in the absence of the external field ($|\mathbf{H}_{ex}| = 0$), ${w_r}^0/2\pi = 0.68$ GHz (same as in ref. 12). Below we also consider the dynamics of composites filled with iron oxide nanoparticles (magnetite, or Fe_3O_4). For these composites, we set $w_m/2\pi = 19.2$ GHz, $M_s = 4.8 \times 10^5$ A m^{-1}, and $H_a = 0$ (see ref. 12). In this case, we consider two values of the external field $\mu_0|\mathbf{H}_{ex}| = 0.3$ T and $\mu_0|\mathbf{H}_{ex}| = 0.5$ T, setting ${w_r}^0/2\pi = 3.1$ GHz and ${w_r}^0/2\pi = 9.6$ GHz for these external fields, respectively.

For the relative permittivity of a medium (PNIPAAm), we set $\varepsilon_{eff} = 70$.[49] Notably, the variations in ε_{eff} remain small around the volume phase transition,[49] so that these variations could be neglected. The phenomenological damping coefficient α is measured experimentally and typically ranges[50] from 0.001 to 0.05. Herein, following ref. 12, we set $\alpha = 0.05$.

For the properties of the hydrogel matrix, we chose the volume fraction of the polymer at preparation and the dimensionless crosslink density as $\varphi_0 = 0.114$ and, $c_0 v_0 = 7.2 \times 10^{-14}$, respectively.[11] For the gel–solvent interaction parameter, we set $\chi_1 = 0.518$ and calculated $\chi_0(T)$ as specified above (eqn (18)) using $\delta h = -12.4 \times 10^{-14}$ and $\delta s = -4.7 \times 10^{-16}$ for the variations in the enthalpy and entropy per monomeric unit of the network based on the respective experimental data for neutral PNIPAAm gels.[11] We then calculate the equilibrium degree of swelling at $T^{ini} = 30$ °C as $\lambda^{ini} = 1.079$, and correspondingly, the equilibrium polymer volume fraction, $\varphi^{ini} = 0.09$. We set the initial volume fraction of nanoparticles as $\psi^{ini} = \xi_m\varphi^{ini}$ by choosing $\xi_m = 0.1$ in the reference case. Below, we also vary (decrease) the initial volume fraction of the nanoparticles to probe the effects of their concentration on gel deformations driven by the application of an EM signal.

Taking the dimensionless units of length in our simulations to be $L_0 = 7 \times 10^{-7}$ m, we can relate the initial dimensional thickness of the gel to the dimensional value of $d_0 = d^{ini}L_0 \approx 5.3$ microns, where $d^{ini} = (L_z - 1)\lambda^{ini}$ is the initial dimensionless thickness of the sample, with the sample size taken as $8 \times 8 \times 8$ nodes. The characteristic time scale can be estimated as[35] $\tau_0 \approx {d_0}^2/D$, where D is the collective diffusion coefficient for the polymer gel matrix. Choosing $D = 2 \times 10^{-11}$ m^2 s^{-1} (ref. 35) and relating the dimensional characteristic relaxation time for this sample to the dimensionless relaxation time, which we calculate from the simulations as $\tau \approx 4.0$, we estimate the characteristic time scale[51] as $T_0 = 0.3$ s. The dimensionless angular frequency in the simulations below is scaled with $W_0 = 2\pi \times 10^9$ Hz.

Finally, to calculate the heating rate in eqn (5), we probe two values of the power density of the incident EM wave. For the majority of runs, we set $P_0 \approx 0.5$ kW m^{-2}, which is twice lower than the value used in ref. 12 and lower than the power density of sunlight. This value, however, significantly exceeds the power densities used in the wireless communication systems. In a separate simulation run, we also show that even using significantly lower power density, $P_0 \approx 10$ W m^{-2}, results in the same behaviour but correspondingly scaled with time. We have chosen this specific low value of the power density since this is the maximum power density for the millimeter-wave signals for frequencies between 6 and 100 GHz required by the Federal Communication Commission (FCC).[52] Finally, for simplicity, we use specific heat capacity of water, $c_p = 4185.5$ J (kg K)$^{-1}$; however, our additional simulations show that accounting for the contributions from both the polymer and water to c_p as the polymer volume fraction varies during phase transitions even further amplifies the heating rate. We take the density of the water–gel system as 10^3 kg m^{-3}.

3. Results and discussion

We now utilize the M-gLSM approach developed above to focus on the mechanical response of the gel composite to the applied EM waves of various frequencies. We begin with the application of the EM wave with three different frequencies (Fig. 2a) for a fixed duration of time (10^3 dimensionless time units, which is approximately equal to 5 min with the above scaling). Initially, all the samples are identical with the volume fractions of nanoparticles set to $\psi = 9 \times 10^{-3}$. The initial sample is shown in Fig. 2b, snapshot I; the color in Fig. 2b represents the volume fraction of the polymer, φ, with the green color corresponding to the lowest and the violet color to the highest value of φ, respectively.

For the applied dimensionless frequency $w = 32.0$, the temperature increases nearly linearly within the time interval considered in the simulations (green line in Fig. 2a). This corresponds to the approximately constant values of the absorption coefficient, η, at this frequency (see Fig. S1a of ESI,† green line), a small decrease in the sample thickness (green line in Fig. S1b, ESI†) and a small increase in the volume fraction of the nanoparticles (green line in Fig. S1c of the ESI†). In this case, the sample behaviour is similar to that of the non-deformable composite under the FMR heating[12] with the small deviations caused by the shrinking or the composite.

For the remaining two frequencies of the EM signal chosen in Fig. 2a, we observe a sharp increase in the heating rate with time (see also the remaining two curves in Fig. S1, ESI†), resulting in a nonlinear increase in temperature; this increase takes place at different instants in time occurring at an earlier time for $w = 27.4$ (red curve) than for $w = 26.7$ (black curve). The snapshots in Fig. 2b(I–IV) correspond to different times along the red curve in Fig. 2a and clearly show that the application of the EM wave at this frequency results in the fastest shrinking of the sample. The three different frequencies considered herein result in distinctly different rates of heating and, correspondingly, distinctly different degrees of swelling by the end of the simulations runs (at $t = 10^3$), as can be seen by comparing the morphologies of the samples corresponding to the final snapshots in these simulations for the red, black and green curves (see snapshots shown in Fig. 2b(IV–VI)). Furthermore, in the additional simulation run (Fig. S2 of ESI†), we show that using a significantly lower power density, $P_0 = 10$ W m^{-2} (see Section 2.3 above), results in the same behavior but correspondingly scaled with time. Since the heating rate is proportional to P_0, using low power density correspondingly slows down the volume phase transition, but all the features of the dynamics and the gel morphology at the correspondingly rescaled time of the signal application remain the same (Fig. S2 of the ESI†). We note that in our simulations, we use cubic samples of size $8 \times 8 \times 8$ nodes (notations are defined in ref. 36); the corresponding dimensional size of this sample can be recalculated as 5.3 μm × 5.3 μm × 5.3 μm (details are given in Section 2.3). This sample is a good representation of the gel film with significantly larger lateral dimensions and the same thickness d sliding along the bottom substrate, as shown in Fig. S3 of the ESI.† This figure shows that the dynamics of the volume phase transition of the 5.3 μm × 5.3 μm × 5.3 μm and 10.6 μm × 10.6 μm × 5.3 μm samples are identical under the EM irradiation. Thus, taking the distribution of the magnetic field uniform as that in a film, one can get a good representation of the gel film with significantly larger lateral dimensions and the same thickness d sliding along the substrate.

To understand the physical origin of the behavior observed in Fig. 2a and b, we now plot the polymer volume fraction, φ, for the same simulation runs (Fig. 2c). The red curve in Fig. 2c shows a distinct increase at $t \approx 500$ dimensionless time units (red curve at $w = 27.4$). Recall that the concentration of the nanoparticles is proportional to the polymer volume fraction, φ, because the nanoparticles are assumed to remain trapped within the polymer matrix. Hence, this increase in nanoparticles concentration results in an increase in the absorption

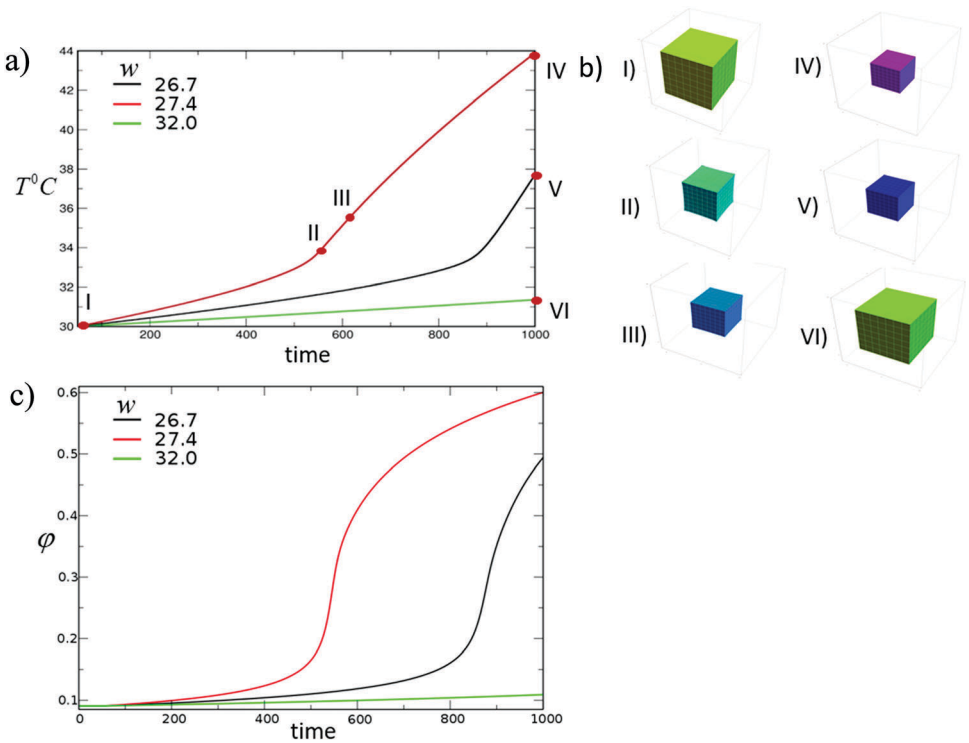

Fig. 2 (a) Absorption coefficient η as a function of time for three normalized frequencies as given in the legend. (b) Gel morphologies at times marked as I-VI in (a). (c) The time evolution of the volume fraction of nanoparticles, ψ, for the same simulation runs as given in (a).

coefficient at this time instant (see a sharp increase in absorption coefficient in Fig. S1a, ESI†) and a corresponding sharp increase in temperature T at the same time as observed in Fig. 2a. A similar sharp increase in φ, but at a later instant in time, is observed for the second scenario (black curve that corresponds to w = 26.7 in Fig. 2c and Fig. S1a–c, ESI†). Finally, at w = 32.0, an increase in φ remains insignificant and approximately linear within the considered simulation time frame (green line in Fig. 2c).

In Fig. 3 we plot the data from the same simulations as in Fig. 2a and c but now we calculate the corresponding degree of swelling, $\lambda(T)$, for each instant in time for all three cases (see eqn (19)). This plot illustrates that all the curves overlap following the same volume phase transition curve; however, the applied frequency defines the point on this curve that is reached during the fixed time interval the signal is applied. The blue arrow on this plot shows the direction of time, and the filled circles of the corresponding color mark the degree of swelling at a given frequency after the application of the signal for the chosen fixed duration of time ($t = 10^3$, corresponding to approximately 5 min). In other words, the circles correspond to the final simulation points shown in Fig. 2a.

While the red curve in Fig. 2a exhibits a steep increase upon initial shrinking close to the volume phase transition temperature caused by an increase in the concentration of nanoparticles, this increase in temperature becomes less pronounced (the slope of the curve drops) with an even further increase in ψ. In other words, we observe an amplification of the heating rate upon the increase in nanoparticle concentration but only until this concentration reaches some critical value. This behaviour is clearly seen in the corresponding time evolution plots of the absorption coefficient, η (red and black curves in Fig. S1a, ESI†), and in the inset in Fig. 4a.

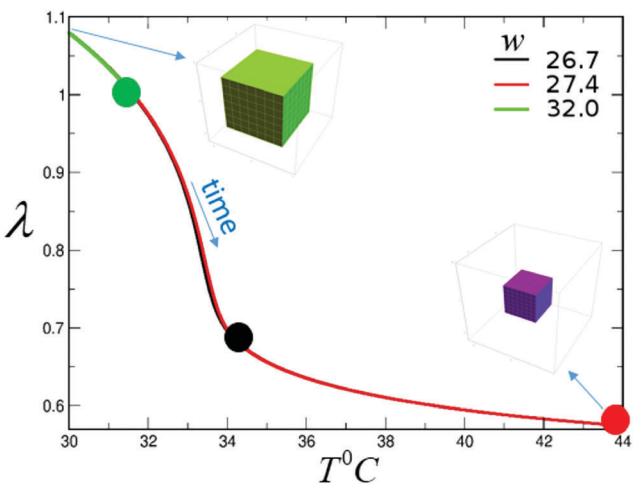

Fig. 3 The degree of swelling of the gel-based composite, λ, as a function of its temperature at three different normalized frequencies as given in the legend. The blue arrow shows the direction of time, and the green, black, and red filled circles mark the points on the volume phase transition curve that are reached at a given applied frequency (w = 32.0, w = 26.7, and w = 27.4, respectively) after the signal was applied for a fixed duration of time ($t = 10^3$).

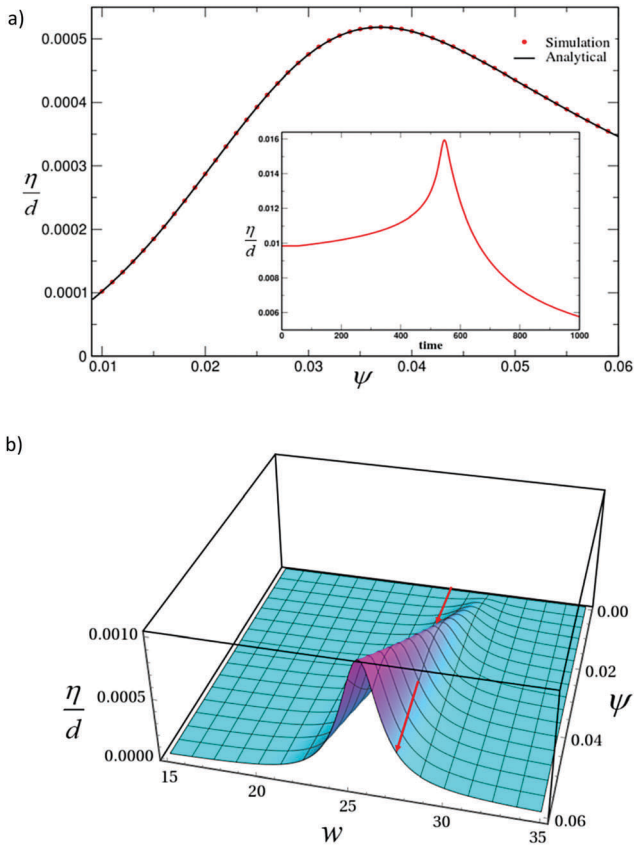

Fig. 4 (a) Absorption coefficient normalized by the thickness of the gel (η/d) as a function of the volume fraction of nanoparticles, ψ, for w = 27.4. The red dots represent simulation data and the continuous black curve corresponds to the analytical calculations. The inset shows η/d from the same simulation run as a function of time; (b) surface plot of η/d as a function of the incident normalized frequency, w, and the volume fraction of nanoparticles, ψ. The cross-section of the surface plot taken at w = 27.4 (marked by the red arrows) represents the solid black curve in (a).

To understand this behavior, in Fig. 4a we plot η/d (red dots) as a function of nanoparticles concentration, ψ (the evolution of ψ during the same run is shown in Fig. S1c, ESI,† red curve). We note that η/d is chosen here to characterize the system's behaviour, since η/d has only a weak dependence on the thickness d, which could be neglected in the analysis, while η does depend on d strongly (see Fig. S1a, ESI†). Furthermore, η/d defines the heating rate (see eqn (4) above). While the red dots in Fig. 4a correspond to the simulation data (simulation run shown by red curves in Fig. 2a and c), the black line is calculated using analytical expressions above (eqn (5)) in the limiting cases, where d and ψ are chosen manually rather than taken from the simulations during the volume phase transitions.

An increase in the absorption coefficient with an increase in nanoparticles concentration is anticipated, and hence the drop observed in η/d at relatively high values of ψ in Fig. 4a appears somewhat counterintuitive. This peak is also clearly apparent in the time evolution plot of η/d in the inset in Fig. 4a. An existence of this peak could be understood when the dependence of the η/d on both, the frequency of the applied signal, w, and nanoparticles concentration, ψ, is considered simultaneously

using eqn (5) (see Fig. 4b). The position of this peak is given by eqn (3); the resonance frequency is higher for low concentrations of nanoparticles and linearly decreases with an increase in ψ (the peak shifts to the left at higher ψ in the three-dimensional surface plot in Fig. 4b). If we follow the maximum peak values of η/d along the surface plot in Fig. 4b by changing the frequency of an incident EM signal, w, to stay at the resonance frequency at any given concentration of ψ, the highest absorption rates are observed, as anticipated, at the highest concentration of nanoparticles. In other words, the height of the peak in Fig. 4b increases with the increase in ψ with the corresponding variation in w to stay at the resonance frequency for each value of ψ. If, on the other hand, we keep an incident frequency w constant and, for example, follow the arrows for w = 27.4 in Fig. 4b, we find that the height of the peak first increases then decreases, which is identical to the behavior observed in our simulations. The solid curve in Fig. 4a represents the cross-section of the surface plot in Fig. 4b taken at w = 27.4 (analytical calculations); an overlap between the simulation results (circles in Fig. 4a) and an analytical curve confirms the numerical accuracy of integrating the electrodynamic equations (given in Section 2.1) using M-gLSM.

In the next series of simulations, we characterize the sample temperature, T, and its mechanical feedback through its thickness, d, by applying an EM wave with a range of frequencies for a fixed time period of $t = 10^3$. The blue curves in Fig. 5a and b show the final temperature and thickness of the sample for these frequencies at $t = 10^3$, while black and red curves show sample's temperature at earlier times as marked in the legend. Note that at the frequency w = 27.4 selected in one of the examples in Fig. 2, the maximum temperature is reached within this time frame. The temperature of the sample decreases with either an increase or a decrease in incident frequency with respect to this critical frequency at a given time, with negligibly small heating for the frequencies significantly higher or lower than this value.

We emphasize the asymmetric nature of the bell-shaped curve in Fig. 5a (blue curve), which can be understood from eqn (3) that gives the value of the resonance frequency, w_c. As the system undergoes volume phase transition, an increase of the volume fraction of the nanoparticles (proportional to the volume fraction of the polymer) causes a decrease of the resonance frequency with time (see eqn (3) and the surface plot in Fig. 4b). Hence, the resonance frequency, w_c, is a variable and not a constant value that depends on the degree of swelling of the sample. Correspondingly, during early times, as long as shrinking is relatively insignificant (black curve in Fig. 5a), the bell-shaped curve is nearly symmetric. At later times, a resonance frequency shifts towards lower values (red and blue curves, respectively). Recall that the sample's temperature measured at given times accounts for the contributions of the temperature increments during the entire heating process as the sample undergoes phase transition.

Our results show different feedback mechanisms in these composites. For a wide range of system parameters, the positive feedback mechanism dominates: magnetic heating increases

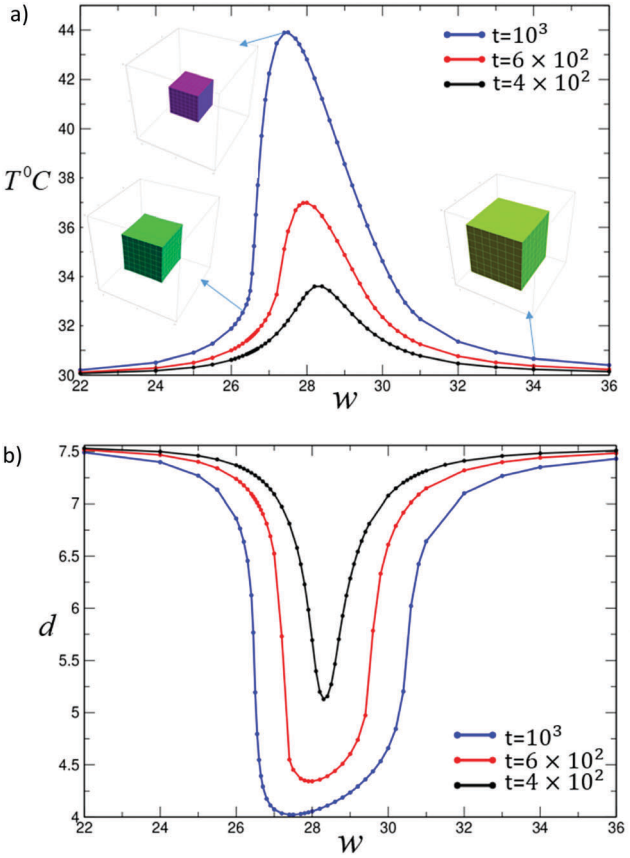

Fig. 5 (a) Temperature as a function of applied frequency, w, for the duration of FMR heating $t = 4 \times 10^2$ (black curve), 6×10^2 (red curve) and 10^3 (blue curve). The images in the inset show composites at the time instances as marked by the arrows. (b) The thickness of the film as a function of applied frequency, w, for the simulation runs in (a).

the volume fraction of nanoparticles *via* gel shrinking, correspondingly increasing the heating rate. However, a negative feedback mechanism is also observed: at some conditions, magnetic heating increases the volume fraction of nanoparticles *via* gel shrinking beyond some peak value of ψ, and the EM wave frequency in these cases is shifted significantly from the resonance frequency so that the further increase leads to the decrease in the heating rate (Fig. 4).

In our next set of simulations (Fig. 6), we vary the initial volume fraction of nanoparticles from 4.5×10^{-3} (red curve) to 6.3×10^{-3} (black curve) to 9×10^{-3} (blue curve, our reference case). The plot in Fig. 6 shows that, as could be anticipated from eqn (3), the peak value in the sample's temperature for the highest concentration of nanoparticles, ψ (blue curve), is located at a lowest frequency (compared to that for the remaining values of NP concentrations). The asymmetry of the bell-shaped curves can again be understood from eqn (3) that allows us to determine the apparent critical frequency. Note the existence of a range of frequencies at which the application of a signal for this time interval shows distinctly different sample temperatures for different initial concentrations of nanoparticles (one such example is indicated by vertical dashed line at w = 27.4 in Fig. 6). However, at certain values of applied w the heating and,

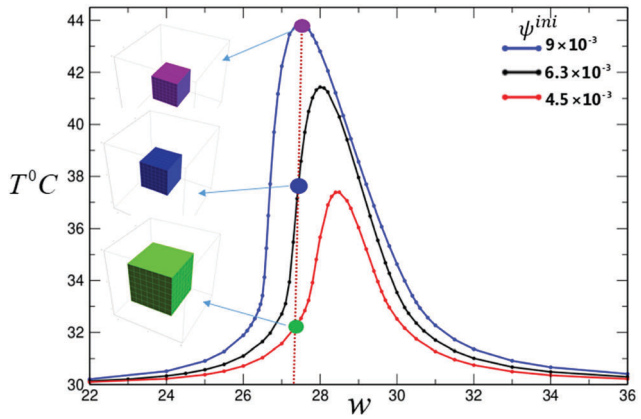

Fig. 6 The temperature of the composite as a function of applied frequency, w, for the dimensionless duration of FMR heating ($t = 10^3$) at different initial volume fractions of nanoparticles: $\psi_{int} = 9 \times 10^{-3}$ (blue curve), 6.3×10^{-3} (black curve), and 4.5×10^{-3} (red curve). The images in the inset show the composites at the frequency $w = 27.4$.

correspondingly, the mechanical response would be similar for the samples with different volume fractions of nanoparticles (see, for example, nearly overlapping regions on the blue and black curves in Fig. 6). The nonlinear effects discussed above are the cause of these closely matching responses for different samples.

In the final series of simulations, we probe the dynamical response of the composites filled with iron oxide nanoparticles (magnetite, Fe_3O_4). Magnetite nanoparticles are often used as magnetic fillers since they are biocompatible and inexpensive and have a good colloidal stability.[53] Fig. 7a shows the temperature of the composite under FMR heating with a fixed initial concentration of nanoparticles (9×10^{-3}) placed in the external fields of $\mu_0|\mathbf{H}_{ex}| = 0.3$ T (black curve) and $\mu_0|\mathbf{H}_{ex}| = 0.5$ T and (blue curve). The remaining modelling parameters are set as provided in Section 2.3 above. As can be anticipated from eqn (3), the resonance frequency is shifted towards the right in a higher external field (blue curve). Similar to the simulations shown in Fig. 5a, we applied the EM signal for the same duration of time (10^3 dimensionless units, corresponding to 5 min with the scaling given in Section 2.3). The heating rate in these iron oxide nanoparticles, however, is significantly lower,[12] than that in Co nanoparticles, and hence our simulations show that this time interval is not sufficient to drive the sample through the volume phase transitions. We also note the symmetry of the bell-shaped curves in Fig. 7a: again, this is due to the relatively small degree of shrinking of the sample during this time interval and, correspondingly, small increases in nanoparticles volume fractions. Upon the application of the EM signal during twice longer time interval (red curve in Fig. 7b), the sample undergoes volume phase transitions (see Fig. S4, ESI†) and the asymmetry of the bell-shaped curve becomes apparent with the critical frequency shifted to the left as in the previous scenario of Co nanoparticles. These results show that the observed behavior is robust and can be anticipated for various types of nanoparticle.

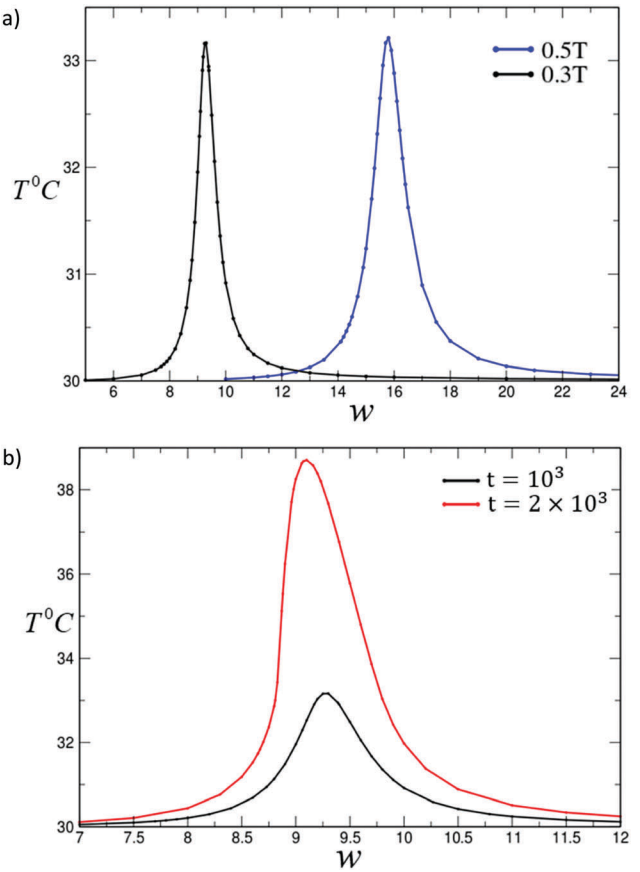

Fig. 7 (a) The temperature of the PNIPAAm–Fe_3O_4 composite as a function of applied frequency, w, for the dimensionless time of FMR heating ($t = 10^3$) at volume fractions of nanoparticles $\psi_{int} = 9 \times 10^{-3}$ and at $\mu_0|\mathbf{H}_{ex}| = 0.3$ T (black curve) and $\mu_0|\mathbf{H}_{ex}| = 0.5$ T (blue curve). (b) The temperature as a function of applied frequency, w, for the dimensionless time of heating $t = 10^3$ (blue curve) and $t = 2 \times 10^3$ (red curve) at $\mu_0|\mathbf{H}_{ex}| = 0.3$ T.

4. Conclusions

Using computational modeling, we focus on soft gel-based composites formed by a thermo-responsive gel filled with uniformly dispersed magnetic nanoparticles. We assume that nanoparticles remain trapped within the polymer matrix and show that these composites undergo large scale elastic deformations upon electromagnetic heating within the GHz frequency range. To model this system, we extended the 3D gLSM approach capturing gel elastodynamics[36] to account for the FMR heating[12] of the gel composite due to the partial absorption of the energy of the incident EM wave; we refer to this extended model as M-gLSM model. During the application of the EM irradiation, the size of the sample and the volume fraction of the nanoparticles vary with time as the sample shrinks due to the heating; correspondingly, the heating rate as well as magnetic permittivity changes dynamically, which is accounted for in our model.

Our results show that the heating rate is highly selective to the frequency of the incident EM signal and is nonlinearly coupled with the gel's dynamics. We isolate a range of conditions

at which large-scale deformations of the gel composite are observed in response to the relatively small variation of the applied EM signal. Importantly, the resonance frequency, w_c, depends on the nanoparticles concentration and is a variable and not a constant value in this system. Hence, the resonance frequency depends on the degree of swelling of the composite, resulting in the dependence of the sample's characteristic response on the time of application of the EM signal. Specifically, at early times, the sample's temperature as a function of incident frequency is a nearly symmetric bell-shaped curve with a maximum at a resonance frequency. At later times, however, as the shrinking of the sample becomes more pronounced, the resonance frequency shifts towards lower values, so that the bell-shaped curve with the maximum at a resonance frequency becomes asymmetric.

We observe both positive and negative feedback mechanisms in these composites. For a range of parameters, the positive feedback mechanism dominates: magnetic heating increases the volume fraction of nanoparticles *via* gel shrinking, correspondingly increasing the heating rate. However, a negative feedback mechanism is also observed when magnetic heating increases the volume fraction of nanoparticles *via* gel shrinking beyond the peak value of volume fraction of nanoparticles, shifting the resonance frequency sufficiently far from the frequency of the incident signal. Furthermore, we show that varying the initial volume fraction of nanoparticles results in distinctly different magnitudes of the mechanical response of the system, allowing one to tailor the system's response by choosing the initial volume fraction of nanoparticles and by varying the frequency of the incident signal or the magnitude of the applied bias field.

In the above studies, we focused our attention on small cubic samples; this geometry represents an ideal reference case for the study of coupling between mechanical feedback and selective FMR heating in these composites. We note, however, that the developed M-gLSM framework readily allows one to account for the magnetic heating and non-uniform deformations of the spatially extended samples. Furthermore, it would be instructive to account for the contributions from the dielectric losses for spatially extended samples to capture the EM heating for a range of composites potentially used as soft active elements of actuators in a wide variety of conditions beyond the conditions considered in the above simulations. To account for the component of the heating rate due to the dielectric losses, the M-gLSM framework developed herein needs to be further extended. Further extensions of the developed computational framework will also include relaxing the requirement of thermal insulation and accounting for the different heat exchange conditions with the surrounding medium.

Herein, we considered two types of nanoparticles dispersed within the polymer matrix: cobalt and iron oxide (magnetite) nanoparticles. Magnetite nanoparticles have a number of advantages since they are inexpensive and biocompatible, and have a good colloidal stability;[53] these nanoparticles are widely used in different applications ranging from MRI imaging to magnetic recording.[54] We have shown that the main features of the system's mechanical response (high selectivity and a shift towards lower resonance frequencies as the gel undergoes volume phase transition) remain qualitatively the same for both types of nanoparticles, while the actual magnitude of the effect and the value of the resonance frequency strongly depend on the chemical nature of the nanoparticles. Hence one can tailor the composite's response by varying the chemical nature of the nanoparticles or by using mixtures of magnetic nanoparticles. Furthermore, while in our studies we choose PNIPAAm gels as our reference system, we anticipate that a similar mechanical response will be observed for a range of gels filled with nanoparticles, for example for poly(*N*-vinylcaprolactam) (PVCL) gels. The PVCL gels are stable against hydrolysis, biocompatible and exhibit volume phase transitions nearly identical to that in PNIPAAm gels.[55]

In summary, our results show that the interactions of the EM signal with the gel composites drive the volume phase transitions and result in large-scale mechanical responses of the samples for a range of applied frequencies. This response depends on the initial concentration of nanoparticles and their chemical nature, and can be regulated dynamically by changing the frequency of the incident EM signal, the time of the application of this signal, or the external bias field. We show that these systems exhibit high selectivity to the frequency of the incident EM signal. Our results suggest a new approach to design active gel-based composites that could be used in a range of soft actuators remotely controlled by the low power EM signals within the GHz frequency range.

Conflicts of interest

There are no conflicts of interest to declare.

Acknowledgements

The authors acknowledge Dr Yu Gu, Mr Chinmay Sonar and Mr Yao Xiong for useful discussions. OK gratefully acknowledges the National Science Foundation EPSCoR Program under NSF Award # OIA-1655740 for partial financial support of O. S. and the National Science Foundation DMR Award #1460836 for financial support of T. M.

References

1 S. M. Palak, P. Parikh and M. G. Kanabar, IEEE, 2010.
2 M. Lapine, I. V. Shadrivov, D. A. Powell and Y. S. Kivshar, *Sci. Rep.*, 2011, **1**, 138.
3 M. Lapine, I. V. Shadrivov, D. A. Powell and Y. S. Kivshar, *Nat. Mater.*, 2012, **11**, 30–33.
4 P. Ilg, *Soft Matter*, 2013, **9**, 3465–3468.
5 R. Weeber, S. Kantorovich and C. Holm, *Soft Matter*, 2012, **8**, 9923–9932.
6 Y. L. Raikher and O. V. Stolbov, *J. Magn. Magn. Mater.*, 2003, **258**, 477–479.
7 R. Weeber, M. Hermes, A. M. Schmidt and C. Holm, *J. Phys.: Condens. Matter*, 2018, **30**, 063002.

8 E. S. Minina, P. A. Sanchez, C. N. Likos and S. S. Kantorovich, *J. Magn. Magn. Mater.*, 2018, **459**, 226–230.
9 R. Weeber, P. Kreissl and C. Holm, *Arch. Appl. Mech.*, 2018, 1–14.
10 M. Zrinyi, L. Barsi and A. Buki, *J. Chem. Phys.*, 1996, **104**, 8750–8756.
11 S. Hirotsu, *J. Chem. Phys.*, 1991, **94**, 3949–3957.
12 Y. Gu and K. G. Kornev, *J. Appl. Phys.*, 2016, **119**, 095106.
13 S. Campbell, D. Maitland and T. Hoare, *ACS Macro Lett.*, 2015, **4**, 312–316.
14 V. A. J. Silva, P. L. Andrade, M. P. C. Silva, A. Bustamante D, L. De Los Santos Valladares and J. Albino Aguiar, *J. Magn. Magn. Mater.*, 2013, **343**, 138–143.
15 C. Gollwitzer, A. Turanov, M. Krekhova, G. Lattermann, I. Rehberg and R. Richter, *J. Chem. Phys.*, 2008, **128**, 164709.
16 S. B. Campbell, M. Patenaude and T. Hoare, *Biomacromolecules*, 2013, **14**, 644–653.
17 F. Reyes-Ortega, Á. Delgado, E. Schneider, B. Checa Fernández and G. Iglesias, *Polymers*, 2017, **10**, 10.
18 A. Seki, E. Kita, D. Isaka, Y. Kikuchi, K. Z. Suzuki, A. Horiuchi, M. Kishimoto, H. Yanagihara, T. Oda, N. Ohkohchi, H. Ikehata and I. Nagano, *J. Phys.: Conf. Ser.*, 2014, **521**, 012014.
19 S. Tong, C. A. Quinto, L. Zhang, P. Mohindra and G. Bao, *ACS Nano*, 2017, **11**, 6808–6816.
20 A. G. Kolhatkar, A. C. Jamison, D. Litvinov, R. C. Willson and T. R. Lee, *Int. J. Mol. Sci.*, 2013, **14**, 15977–16009.
21 J. Pearce, A. Giustini, R. Stigliano and P. Jack Hoopes, *J. Nanotechnol. Eng. Med.*, 2013, **4**, 110071.
22 M. Häring, J. Schiller, J. Mayr, S. Grijalvo, R. Eritja and D. Díaz, *Gels*, 2015, **1**, 135–161.
23 Z. Q. Zhang and S. C. Song, *Biomaterials*, 2016, **106**, 13–23.
24 X. Lin, R. Huang and M. Ulbricht, *J. Mater. Chem. B*, 2016, **4**, 867–879.
25 K. L. Ang, S. Venkatraman and R. V. Ramanujan, *Mater. Sci. Eng., C*, 2007, **27**, 347–351.
26 N. S. Satarkar and J. Z. Hilt, *J. Controlled Release*, 2008, **130**, 246–251.
27 M. K. Jaiswal, R. Banerjee, P. Pradhan and D. Bahadur, *Colloids Surf., B*, 2010, **81**, 185–194.
28 R. Hernańdez, J. Sacristań, L. Asıń, T. E. Torres, M. R. Ibarra, G. F. Goya and C. Mijangos, *J. Phys. Chem.*, 2010, **114**, 12002–12007.
29 T. L. Gilbert, *IEEE Trans. Magn.*, 2004, **40**, 3443–3449.
30 A. Arbe, P. Malo de Molina, F. Alvarez, B. Frick and J. Colmenero, *Phys. Rev. Lett.*, 2016, **117**, 185501.
31 J. A. Pearce, J. R. Cook, P. J. Hoopes and A. Giustini, *Proc. SPIE-Int. Soc. Opt. Eng.*, 2011, **7901**, 1–6.
32 J. R. C. John, A. Pearce and S. Y. Emelianov, IEEE, 2010.
33 L. D. Landau and E. M. Lifshitz, *Electrodynamics of continuous media*, Pergamon Press, Oxford, New York, 2nd edn, 1984.
34 A. Suzuki and T. Tanaka, *Nature*, 1990, **346**, 345–347.
35 H. Hirose and M. Shibayama, *Macromolecules*, 1998, **31**, 5336–5342.
36 O. Kuksenok, V. V. Yashin and A. C. Balazs, *Phys. Rev. E: Stat., Nonlinear, Soft Matter Phys.*, 2008, **78**, 041406.
37 V. V. Yashin and A. C. Balazs, *J. Chem. Phys.*, 2007, **126**, 124707.
38 V. V. Yashin, O. Kuksenok and A. C. Balazs, *Prog. Polym. Sci.*, 2010, **35**, 155–173.
39 R. Yoshida, *Adv. Mater.*, 2010, **22**, 3463–3483.
40 I. C. Chen, O. Kuksenok, V. V. Yashin, R. M. Moslin, A. C. Balazs and K. J. Van Vliet, *Soft Matter*, 2011, **7**, 3141–3146.
41 O. Kuksenok, V. V. Yashin, M. Kinoshita, T. Sakai, R. Yoshida and A. C. Balazs, *J. Mater. Chem.*, 2011, **21**, 8360–8371.
42 R. Yoshida, M. Tanaka, S. Onodera, T. Yamaguchi and E. Kokufuta, *J. Phys. Chem. A*, 2000, 7549–7555.
43 P. Yuan, O. Kuksenok, D. E. Gross, A. C. Balazs, J. S. Moore and R. G. Nuzzo, *Soft Matter*, 2013, **9**, 1231–1243.
44 S. O. Chikazumi and C. D. Graham, *Physics of Ferromagnetism*, Oxford University Press, Oxford, New York, 2nd edn, 2009.
45 D. J. Griffiths, *Introduction to Electrodynamics*, Cambridge University Press, 4th edn, 2013.
46 T. L. Hill, *An Introduction to Statistical Thermodynamics*, Addison-Weley, Reading, MA, 1960.
47 R. J. Atkin and N. Fox, *An Introduction to the Theory of Elasticity*, Longman, New York, 1980.
48 A. Onuki, *Adv. Polym. Sci.*, 1993, **109**, 63–121.
49 W. J. Su, K. S. Zhao, J. J. Wei and T. Ngai, *Soft Matter*, 2014, **10**, 8711–8723.
50 C. Thirion, W. Wernsdorfer and D. Mailly, *Nat. Mater.*, 2003, **2**, 524–527.
51 X. M. He, M. Aizenberg, O. Kuksenok, L. D. Zarzar, A. Shastri, A. C. Balazs and J. Aizenberg, *Nature*, 2012, **487**, 214–218.
52 T. Wu, T. S. Rappaport and C. M. Collins, IEEE International Conference on Communications (ICC), 2015.
53 I. M. Obaidat, B. Issa and Y. Haik, *Nanomaterials*, 2015, **5**, 63–89.
54 H. Nemala, J. S. Thakur, V. M. Naik, P. P. Vaishnava, G. Lawes and R. Naik, *J. Appl. Phys.*, 2014, **116**, 034309.
55 J. Ramos, A. Imaz and J. Forcada, *Polym. Chem.*, 2012, **3**, 852–856.

